Journal of the Optical Society of America A
OPTICS, IMAGE SCIENCE, AND VISION

Scalar approximation of Maxwell equations: derivation and accuracy

PATRICK C. CHAUMET,* GUILLAUME MAIRE, AND ANNE SENTENAC

Institut Fresnel, Aix Marseille Univ, CNRS, Centrale Marseille, Marseille, France
**Corresponding author: patrick.chaumet@fresnel.fr*

Received 26 April 2022; revised 28 June 2022; accepted 28 June 2022; posted 7 July 2022; published 25 July 2022

Replacing Maxwell equations by a scalar wave equation is often used in computational imaging to simulate the light–sample interaction. It significantly reduces the computational burden but provides field maps that are insensitive to the polarization of the incident field, provided the latter is constant throughout the sample. Here, we develop a scalar approximation that accounts for the polarization of the incident field. Comparisons with rigorous simulations show that this approach is more accurate than the classical scalar approximation with similar computational cost.

https://doi.org/10.1364/JOSAA.462034

1. INTRODUCTION

The last 20 years have seen the development of computational optical microscopy for recovering quantitative three-dimensional maps of the sample permittivity with better resolution than standard microscopes. This approach consists in numerically reconstructing the sample from multiple images recorded under various illuminations. It can be found in many different systems, such as optical coherence tomography, optical diffraction tomography, or Fourier ptychography [1–10]. The key point of the numerical reconstruction is the model linking the recorded image to the sample permittivity. When the sample is small (a few wavelengths), it is possible to use a rigorous solver of Maxwell equations for simulating the light–matter interaction [11]. This approach accounts for and takes advantage of the multiple scattering and the vectorial nature of the field in highly contrasted samples [2]. However, in many applications (particularly in the biology domain), the samples are large compared to the wavelength and weakly contrasted. In this case, most reconstruction procedures use approximate methods. Born approximation is adapted to weakly scattering samples. Rytov approximation [12,13] or the beam propagation method (BPM) [14] can deal with larger and more distorting objects but is accurate essentially in the forward direction (corresponding to the transmission imaging configuration) [15]. When multiple scattering is important, several groups have proposed to solve the wave equation using a scalar approximation for the electric field [16–18]. This widespread technique is valid when the sample permittivity varies on a scale larger than the wavelength [19]. It is more computationally intensive than the quasi-analytic formulation of Born or Rytov approximations or the BPMs but significantly less than the rigorous solving of Maxwell equations. It accounts for multiple scattering, and is as accurate in reflection as in transmission configurations, but it implies that the field maps inside isotropic samples are insensitive to the polarization of the incident beam.

In this work, we propose a scalar approximation that accounts for the incident polarization provided the latter is constant throughout the sample. This condition is met, for example, when the sample is illuminated by a collimated beam. After describing the theory, we show with numerical simulations that our approach is more accurate than the classical scalar approximation.

2. SCALAR APPROXIMATION: THEORY

We consider a medium described by its relative isotropic permittivity $\varepsilon(\mathbf{r})$ illuminated by a monochromatic light of wavenumber k_0 radiated from a source $\mathbf{S}(\mathbf{r})$. The electric field $\mathbf{E}(\mathbf{r})$ satisfies the vectorial equation,

$$\boldsymbol{\nabla} \times [\boldsymbol{\nabla} \times \mathbf{E}(\mathbf{r})] - \varepsilon(\mathbf{r}) k_0^2 \mathbf{E}(\mathbf{r}) = \mathbf{S}(\mathbf{r}). \tag{1}$$

If the permittivity varies on a scale much larger than the wavelength, $0 = \boldsymbol{\nabla} \cdot [\varepsilon(\mathbf{r})\mathbf{E}(\mathbf{r})] \approx \varepsilon(\mathbf{r})[\boldsymbol{\nabla} \cdot \mathbf{E}(\mathbf{r})]$, and Eq. (1) simplifies to

$$\boldsymbol{\Delta}\mathbf{E}(\mathbf{r}) + \varepsilon(\mathbf{r}) k_0^2 \mathbf{E}(\mathbf{r}) = -\mathbf{S}(\mathbf{r}), \tag{2}$$

where each field component satisfies an independent scalar equation. We now consider configurations in which the field illuminating the sample, i.e., the field created by $\mathbf{S}$ in absence of the sample, $\mathbf{E}_{\text{ref}}(\mathbf{r})$, is a beam with uniform, possibly complex, polarization $\mathbf{u}$,

$$\mathbf{E}_{\text{ref}}(\mathbf{r}) = e_{\text{ref}}(\mathbf{r})\mathbf{u}, \tag{3}$$

where $\mathbf{u}^* \cdot \mathbf{u} = 1$, a^* being the conjugate of a, and e_{ref} is the reference field complex amplitude.

Typically, this condition is met when the sample is illuminated by a collimated beam as in most optical diffraction tomography experiments [1–4,6,8,14]. In this case, the scalar equations satisfied by the three field components are similar. The field $\mathbf{E}(\mathbf{r})$ will be polarized along $\mathbf{u}$ and its complex amplitude $e(\mathbf{r})$ will not depend on $\mathbf{u}$. Under the classical scalar approximation (CSA), changing the polarization of the beam illuminating the sample will not change the field distribution inside the sample. This property, which is indeed observed in slowly varying media, limits the interest of the scalar wave approximation outside its prescribed validity domain, especially when considering bounded samples whose frontiers correspond to a sudden change of permittivity.

To address this issue, we propose another scalar approximation relying only on the assumption that the field polarization inside the sample is close to that of the illuminating field. Introducing a reference permittivity $\varepsilon_{\text{ref}}(\mathbf{r})$ and a sample permittivity contrast $\chi(\mathbf{r})$ such that $\varepsilon(\mathbf{r}) = \varepsilon_{\text{ref}}(\mathbf{r}) + \chi(\mathbf{r})$, Eq. (1) can be transformed into the volume integral equation,

$$\mathbf{E}(\mathbf{r}) = \mathbf{E}_{\text{ref}}(\mathbf{r}) + k_0^2 \int \overline{\mathbf{G}}(\mathbf{r}, \mathbf{r}')\chi(\mathbf{r}')\mathbf{E}(\mathbf{r}')\mathrm{d}\mathbf{r}', \tag{4}$$

where $\overline{\mathbf{G}}$ is the Green dyadic of the reference medium, $\overline{\mathbf{G}}(\mathbf{r}, \mathbf{r}')\mathbf{p}(\mathbf{r}')$ is the (known) field radiated at $\mathbf{r}$ by a dipole placed at $\mathbf{r}'$ in the reference medium, and $\mathbf{E}_{\text{ref}}$ is the (known) illuminating field created by $\mathbf{S}$ in the reference medium.

This integral equation obtained with Maxwell's equations is the cornerstone of the discrete dipole approximation (DDA) [20–24]. It is solved by discretizing the sample support V_{obj}, i.e., the region where $\chi(\mathbf{r}) \neq 0$, into N small cubic subunits of side d over which the three unknown field components of $\mathbf{E}$ are assumed to be constant and solving the resulting $3N \times 3N$ linear system. The linear system is solved iteratively with a conjugate gradient method [25] with the use of the fast Fourier transform [26]. Once the field inside V_{obj} is known, it can be calculated everywhere using Eq. (4) or its far-field version [27].

To obtain a scalar equation, we assume that for any $\mathbf{r} \in V_{\text{obj}}$, $\mathbf{E}(\mathbf{r}) \approx e(\mathbf{r})\mathbf{u}$ and from the scalar product of Eq. (4) with $\mathbf{u}^*$, we obtain

$$e(\mathbf{r}) = e_{\text{ref}}(\mathbf{r}) + k_0^2 \int g_u(\mathbf{r}, \mathbf{r}')\chi(\mathbf{r}')e(\mathbf{r}')\mathrm{d}\mathbf{r}', \tag{5}$$

where $g_u(\mathbf{r}, \mathbf{r}') = \mathbf{u}^* \cdot \overline{\mathbf{G}}(\mathbf{r}, \mathbf{r}')\mathbf{u}$ varies with $\mathbf{u}$, which implies that the Green function and then the scalar field will depend on the polarization of the incident beam. Note that in Appendix A we establish the differential equation satisfied by $e(\mathbf{r})$.

The time required for solving the scalar linear system Eq. (5) scaling as $N\ln(N)$ is expected to be at least three times shorter than that required for solving the full vectorial system, Eq. (4), which scales as $3N\ln(3N)$, with a storage burden divided by 9 (as in the CSA). Hereafter, the classical scalar approximation will be denoted CSA, while that developed in this paper will be called uGu. It is worth noting that CSA can be solved in the same way as uGu, using the integral equation

$$e(\mathbf{r}) = e_{\text{ref}}(\mathbf{r}) + k_0^2 \int g(\mathbf{r}, \mathbf{r}')\chi(\mathbf{r}')e(\mathbf{r}')\mathrm{d}\mathbf{r}', \tag{6}$$

the only difference laying in $g(\mathbf{r}, \mathbf{r}')$ which is the standard scalar Green function, i.e., $g(\mathbf{r}, \mathbf{r}') = e^{ik_0 R}/(4\pi R)$ with $\mathbf{R} = \mathbf{r} - \mathbf{r}'$ and $R = |\mathbf{R}|$ (for an homogeneous reference medium). Thus CSA and uGu can be implemented easily on the same code by just replacing g by g_u.

3. COMPARISONS BETWEEN THE DIFFERENT SCALAR APPROXIMATIONS

In this section, we simulate the scattering by different samples (spheres and cuboids) illuminated by a collimated beam. The samples are of micrometric size (about 10 wavelengths), and their permittivity is increased to test the robustness of the approximations as the multiple scattering increases. We compare the near field $\mathbf{E}(\mathbf{r})$, $\mathbf{r} \in V_{\text{obj}}$ (field inside the sample) and the far field in the $\mathbf{k}$ direction, $\mathbf{E}(\mathbf{r}) = \frac{e^{ik_0 r}}{r}\mathbf{F}(\mathbf{k})$, where $\mathbf{k} = k_0\mathbf{r}/r$ with $r = \mathbf{r}$, and $\mathbf{r}$ is far from the sample, obtained using the different scalar approximations with that given by the rigorous Maxwell equation solver, DDA [24], through the following errors:

$$\text{Err}_{\text{nf}} = \frac{\int_{V_{\text{obj}}} \|\mathbf{E}_{\text{rig}}(\mathbf{r}) - \mathbf{E}_{\text{approx}}(\mathbf{r})\|\mathrm{d}\mathbf{r}}{\int_{V_{\text{obj}}} \|\mathbf{E}_{\text{rig}}(\mathbf{r})\|\,\mathrm{d}\mathbf{r}}, \tag{7}$$

and for the far field

$$\text{Err}_{\text{ff}} = \frac{\int_{2\pi} \|\mathbf{F}_{\text{rig}}(\mathbf{k}) - \mathbf{F}_{\text{approx}}(\mathbf{k})\|\mathrm{d}\Omega}{\int_{2\pi} \|\mathbf{F}_{\text{rig}}(\mathbf{k})\|\mathrm{d}\Omega}, \tag{8}$$

where the integration is performed over 2π str for $k_z > 0$ or $k_z < 0$. We also study the extinction cross section [21,24,28]

$$C_{\text{ext}} = \frac{k_0}{E_{\text{ref}}^2} \int_{V_{\text{obj}}} \text{Im}\left[\mathbf{E}_{\text{ref}}^*(\mathbf{r}) \cdot [\chi(\mathbf{r})\mathbf{E}(\mathbf{r})]\right]\mathrm{d}r, \tag{9}$$

with $E_{\text{ref}} = |\mathbf{E}_{\text{ref}}|$.

A. Accuracy of the Extinction Cross Section

In this subsection, we compare the extinction cross sections of spheres and cuboids of varying size and permittivity calculated by CSA and uGu to those given by the rigorous electromagnetic approx solver DDA via the relative error $(C_{\text{ext}}^{\text{approx}} - C_{\text{ext}}^{\text{rig}})/C_{\text{ext}}^{\text{rig}}$. The simulations were performed by solving the volume integral equations of DDA Eqs. (4), uGu (5), and CSA (6), with the same discretization mesh, $d = 2a/120$, where a is the radius of the spheres or the largest side of the cuboids.

We first study the extinction cross section for a sphere versus its relative permittivity (Fig. 1) and versus its radius (Fig. 2).

Then we study a cuboid of size (a, b, c), as depicted in Fig. 3, illuminated with a plane wave along the z axis and polarization along x [Fig. 3(a)] or y [Fig. 3(b)]. In Fig. 4 we plot the extinction cross section versus the size of the cuboid for both polarizations.

In general, we observe that while the error of the CSA oscillates and can reach 100% for certain configurations, the estimation of the extinction cross section using uGu is always remarkably accurate (error below 4%). Actually, we tried other samples (aggregates of spheres, inhomogeneous media, metallic and dielectric materials) and could not find any examples (that

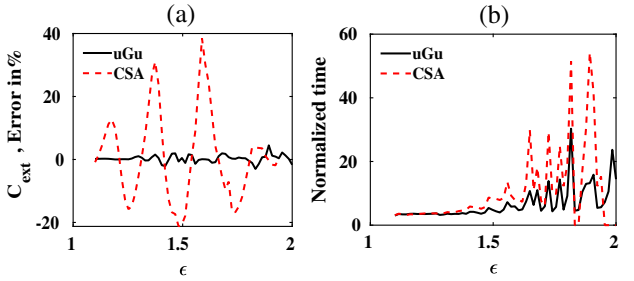

Fig. 1. Extinction cross section versus ε for a sphere of radius $a = 4\ \mu$m illuminated by a plane wave of wavelength 632 nm. (a) Relative error between the CSA, dashed line (uGu, plain line), and the rigorous DDA. (b) Normalized time gain t_{DDA}/t_{CSA} and t_{DDA}/t_{uGu} of the scalar approaches versus the rigorous method.

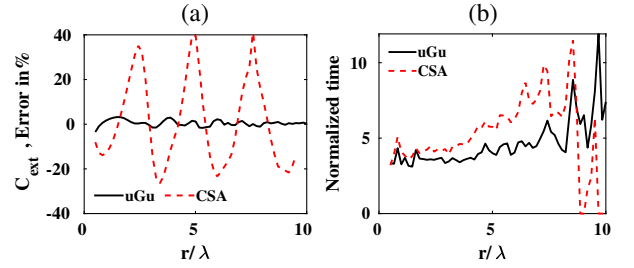

Fig. 2. Same as Fig. 1 but the error is calculated as a function of the radius of the sphere, the relative permittivity being set to $\varepsilon = 1.5$.

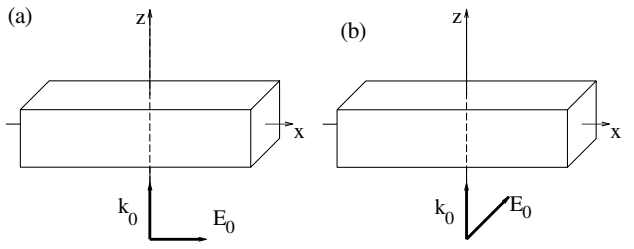

Fig. 3. Representation of a cuboid of sides a and $b = c$ illuminated under normal incidence by a plane wave with different polarizations. (a) Polarization along x axis. (b) Polarization along y axis.

could be handled by the rigorous approach in less than a day) able to challenge the uGu approximation. This striking performance may be explained by noting that the extinction cross section depends only on the field component that is polarized in the same way as the illuminating field. Thus, neglecting the other components, as is done in uGu, has less impact.

The gain in computation time permitted by the scalar approaches was estimated by calculating t_{DDA}/t_{CSA} and t_{DDA}/t_{uGu} and is plotted together with the extinction cross section. As expected, the scalar approaches are significantly faster (by a factor ranging from 3 to 40) than the rigorous method. Most importantly, we observed that the highest time gain was obtained when the rigorous method was particularly slow to converge due to the increasing contribution of multiple scattering (objects of high permittivity and large size); see Ref. [23]. For example, the DDA computation time required for a sphere of radius six wavelengths and permittivity 1.1 was about 5 min and that of uGu about 2 min, but, when the permittivity

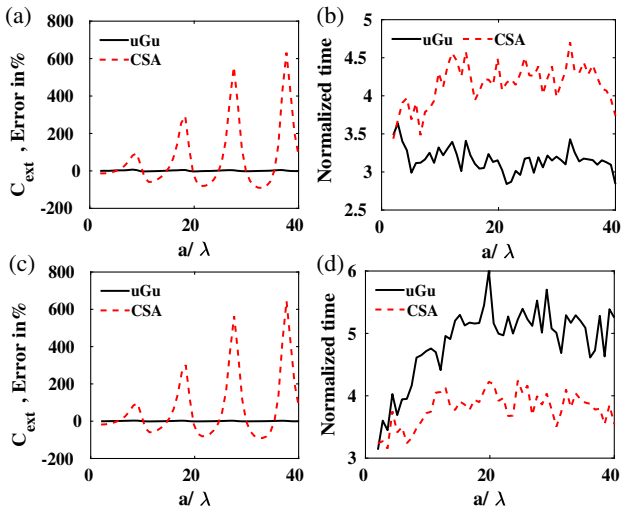

Fig. 4. Extinction cross section as a function of a for a cuboid of dimensions $(a, a/2, a/2)$, as depicted by Fig. 3 for an incident polarization (a), (b) along x and (c), (d) along y. (a), (c) Relative error between the CSA and uGu and the rigorous DDA. (b), (d) Normalized time gain t_{DDA}/t_{CSA} and t_{DDA}/t_{uGu}.

reached 2, the DDA time increased to 2 h while that of uGu remained below 6 min. The uGu gain in computation time can be explained by the fact that its scalar linear system is three-fold smaller than the vectorial one and is also better conditioned. Note that the iterative solving of the uGu linear system always converged while that of the CSA failed for some specific geometries. These cases are indicated by setting to zero the CSA time gain.

B. Accuracy of the Near and Far Fields

In this subsection, we study the accuracy of the near field and the far field estimated by the scalar approaches for a cuboid of size $a = 5\ \mu$m, $b = c = 1\ \mu$m illuminated by a plane wave of $1 = 632.8$ nm. Here, the meshsize is set to $d = a/150$.

Figure 5 shows that uGu is always better than CSA, especially when the polarization of the incident field is along the smallest side of the cuboid. We also observe that the cuboid scatters most of the light in the forward direction; the reflected field is more difficult to estimate than the transmitted one.

To investigate in more detail the behavior of uGu and CSA, we plot in Fig. 6 the amplitude of the near field inside the cuboid for the different incident polarizations. As expected, the field amplitude given by the CSA is the same no matter the incident polarization, whereas those of uGu and DDA differ in the same way. In Fig. 7, we plot the back-scattered field amplitude F for $k_z < 0$ as a function of (k_x, k_y) for the three methods. We have chosen the reflection configuration because the forward-scattered field (transmission configuration) is easier to simulate and approximate methods such as Rytov and BPM are already very efficient for this kind of sample [15]. Once again, we observe that uGu is significantly better than CSA. For the incident polarization along x, uGu is accurate no matter the angles of observation, while for the y polarization, it is accurate for angles close to the specular reflected direction but deteriorates at large angles. On the other hand, CSA fails to recover the

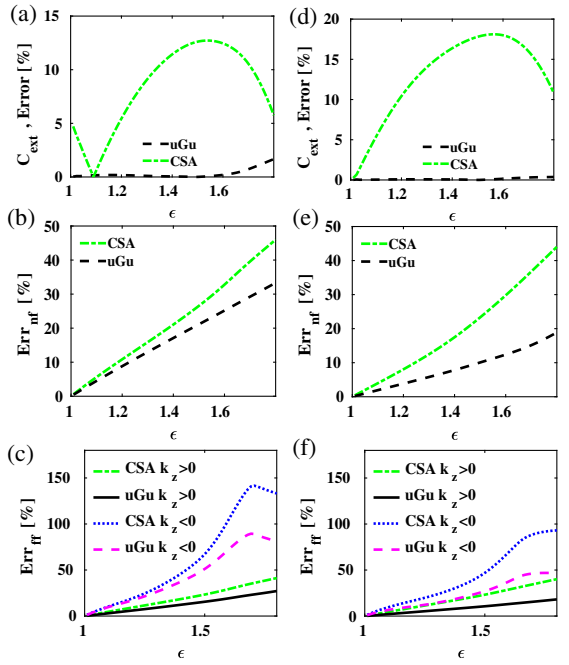

Fig. 5. Relative errors for increasing ε of the extinction cross section (top row), near field (middle row), and far field (bottom row) for a cuboid $a = 5$ μm, $b = c = 1$ μm illuminated by a plane wave with, $1 = 632.8$ nm, x-polarized (left column) or y-polarized (right column). k_z is the z component of the observation wavevector. $k_z > 0$ indicates far-field observation in the transmission configuration (same direction as the incident plane wave), while $k_z < 0$ indicates the reflection configuration.

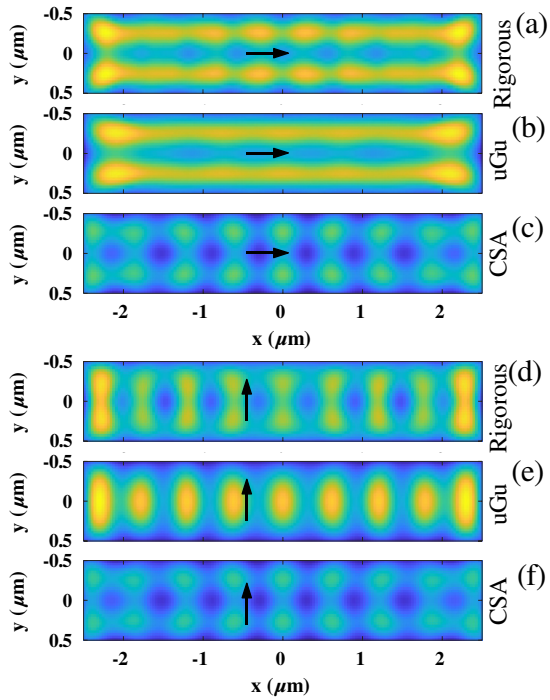

Fig. 6. Near-field amplitude in the (x, y) plane cutting the middle of the cuboid of the configuration depicted in Fig. 3 for an incident polarization along x (first three figures) or along y and $\varepsilon = 1.8$ (last three figures).

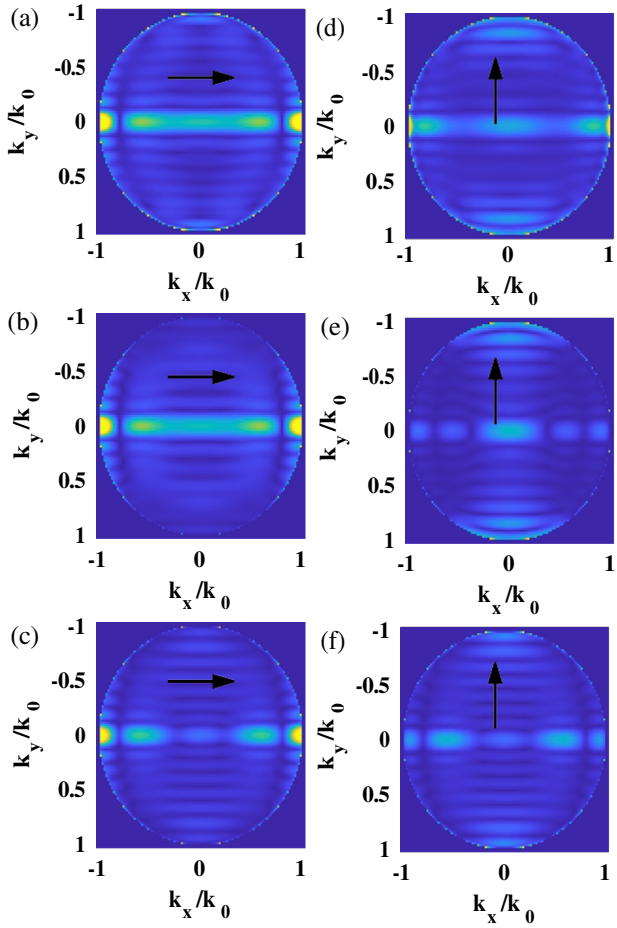

Fig. 7. Back-scattered far-field amplitude in the (k_x, k_y) plane ($k_z < 0$) of the configuration depicted in Fig. 3 for an incident polarization along x (left column) or along y (right column) and $\varepsilon = 1.8$. Top row, rigorous calculation; middle row, uGu; bottom row, CSA.

behavior of the back-scattered far field, the central lobe always being largely underestimated.

4. EXTENDING uGu TO SAMPLES IN MULTILAYER

The uGu method can also be applied to samples placed in a multilayer, as the dyadic Green function of such a reference medium is well known [29] (note that we are not aware of any implementation of the CSA in a multilayered system). However, it requires that the polarization of the reference field be constant throughout the sample for Eq. (3) to be satisfied. This condition is met when the incident beam is polarized parallel to the multilayer interfaces, or if the sample is only illuminated by a transmitted beam (whatever its polarization). Here we consider the same cuboid as in the previous section deposited on a gold substrate and illuminated from vacuum under normal incidence by an x- or y-polarized plane wave. We observe in Fig. 8 that the uGu error in the presence of the substrate is of the same order as that obtained when the cuboid was in vacuum.

The accuracy of uGu is confirmed in Fig. 9, which displays the back-scattered far-field amplitude in the (k_x, k_y) plane for $\varepsilon = 1.6$.

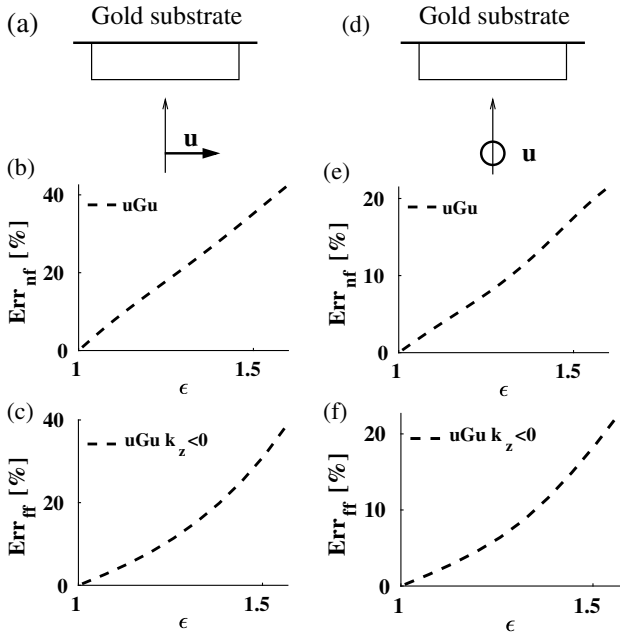

Fig. 8. Error on the near- and far-field uGu simulations for the cuboid of Fig. 3 deposited on a gold interface and illuminated under normal incidence with two polarizations, along x for the left column and along y for the right column. Top row, sketch of the configuration; middle row, near-field error; bottom row, far-field error.

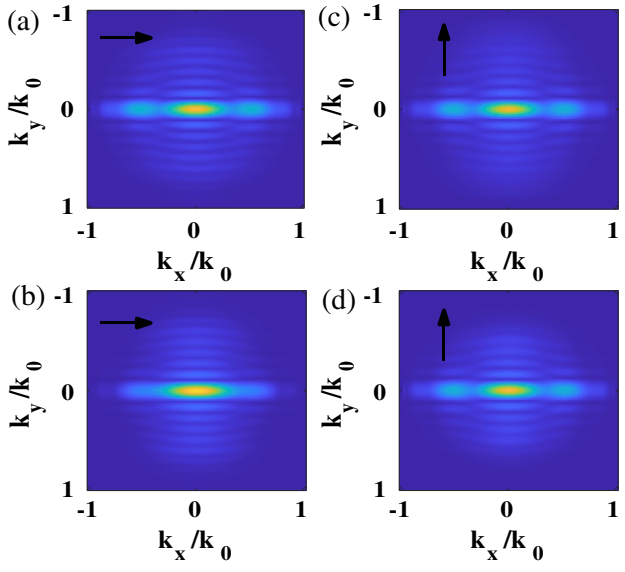

Fig. 9. Back-scattered far-field amplitude in the (k_x, k_y) plane ($k_z < 0$) of the configuration depicted in Fig. 8, with $\varepsilon = 1.6$. Left column, x incident polarization; right column, y polarization. Top row, rigorous calculation; bottom row, uGu.

5. CONCLUSION

In conclusion, we have developed a novel scalar approximation, uGu, which is adapted to configurations where the incident polarization is constant throughout the sample (when the illumination is a collimated beam, for example). No matter the samples considered (and we displayed only a selection of our different tries), uGu was always more accurate than the CSA, with a comparable computation time. Note that the latter is significantly shorter than that of a rigorous calculation (up to 10 times), thanks to the smaller size and better conditioning of the linear system to be solved. In addition, uGu was shown to be particularly adapted to the estimation of the extinction cross section as we could not find one object for which the error exceeded a few percent. Last, uGu was able to reproduce the different behaviors of the near field inside a cuboid when the incident polarization was changed, which could be particularly useful in imaging experiments where different polarizations are used to probe the samples [30,31]. Thus, we believe that uGu should always be preferred to CSA when possible. Note that both the uGu and CSA approximations can be tested in the freely accessible Maxwell equations solver IFDDA and IFDDAM [32].

APPENDIX A: THE DIFFERENTIAL EQUATION OF uGu

The integral equation (5) that is satisfied by the scalar field e is equivalent to a differential equation. Starting from the rigorous vectorial equation

$$\nabla \times [\nabla \times \mathbf{E}(\mathbf{r})] - \varepsilon(\mathbf{r}) k_0^2 \mathbf{E}(\mathbf{r}) = \mathbf{S}(\mathbf{r}), \tag{A1}$$

one obtains

$$\Delta \mathbf{E}(\mathbf{r}) + \varepsilon(\mathbf{r}) k_0^2 \mathbf{E}(\mathbf{r}) = -\mathbf{S}(\mathbf{r}) + \nabla[\nabla \cdot \mathbf{E}(\mathbf{r})], \tag{A2}$$

which, using $0 = \nabla \cdot [\varepsilon(\mathbf{r})\mathbf{E}(\mathbf{r})]$, can be written as

$$\Delta \mathbf{E}(\mathbf{r}) + \varepsilon(\mathbf{r}) k_0^2 \mathbf{E}(\mathbf{r}) = -\mathbf{S}(\mathbf{r}) - \nabla[\nabla \cdot (\chi(\mathbf{r})\mathbf{E}(\mathbf{r}))]. \tag{A3}$$

The classical scalar method amounts to neglecting totally $-\nabla\,[\nabla \cdot (\chi(\mathbf{r})\mathbf{E}(\mathbf{r}))]$ to obtain the three scalar equations,

$$\Delta \mathbf{E}(\mathbf{r}) + \varepsilon(\mathbf{r}) k_0^2 \mathbf{E}(\mathbf{r}) = -\mathbf{S}(\mathbf{r}). \tag{A4}$$

We now assume that $\mathbf{S}(\mathbf{r})$ is a source that creates an incident field that is directed along $\hat{\mathbf{z}}$. The uGu method amounts to approximating $-\nabla[\nabla \cdot (\chi(\mathbf{r})\mathbf{E}(\mathbf{r}))]$ by $-\frac{\partial^2[\chi(\mathbf{r})e(\mathbf{r})]}{\partial z^2}$, where $e(\mathbf{r})$ is the z component of the field. This approximation is justified by the assumption that the x and y components of the field inside the sample (i.e., where $\chi(\mathbf{r}) \neq 0$) are much smaller than the z component. Then the differential equation satisfied by $e(\mathbf{r})$ reads

$$\Delta e(\mathbf{r}) + \varepsilon(\mathbf{r}) k_0^2 e(\mathbf{r}) + \frac{\partial^2[\chi(\mathbf{r})e(\mathbf{r})]}{\partial z^2} = -S_z(\mathbf{r}), \tag{A5}$$

where $S_z(\mathbf{r})$ is the source creating the incident z-polarized field.

Disclosures. The authors declare no conflicts of interest.

Data availability. Data underlying the results presented in this paper are not publicly available at this time, but the IFDDA code under free license is available at [32] and allows one to redo all the calculations presented in this article.

REFERENCES

1. V. Lauer, "New approach to optical diffraction tomography yielding a vector equation of diffraction tomography and a novel tomographic microscope," J. Microsc. **205**, 165–176 (2002).

2. T. Zhang, Y. Ruan, G. Maire, D. Sentenac, A. Talneau, K. Belkebir, P. C. Chaumet, and A. Sentenac, "Full-polarized tomographic diffraction microscopy achieves a resolution about one-fourth of the wavelength," Phys. Rev. Lett. **111**, 243904 (2013).
3. Y. Choi, M. Kim, C. Yoon, T. D. Yang, K. J. Lee, and W. Choi, "Synthetic aperture microscopy for high resolution imaging through a turbid medium," Opt. Lett. **36**, 4263–4265 (2011).
4. M. Debailleul, V. Georges, B. Simon, R. Morin, and O. Haeberlé, "High-resolution three-dimensional tomographic diffractive microscopy of transparent inorganic and biological samples," Opt. Lett. **34**, 79–81 (2009).
5. A. Badon, D. Li, G. Lerosey, A. C. Boccara, M. Fink, and A. Aubry, "Smart optical coherence tomography for ultra-deep imaging through highly scattering media," Sci. Adv. **2**, e1600370 (2016).
6. Y. Park, C. Depeursinge, and G. Popescu, "Quantitative phase imaging in biomedicine," Nat. Photonics **12**, 578–589 (2018).
7. T. S. Ralston, D. L. Marks, P. S. Carney, and S. A. Boppart, "Inverse scattering for optical coherence tomography," J. Opt. Soc. Am. A **23**, 1027–1037 (2006).
8. W. Choi, C. Fang-Yen, K. Badizadegan, S. Oh, N. Lue, R. R. Dasari, and M. S. Feld, "Tomographic phase microscopy," Nat. Methods **4**, 717–719 (2007).
9. G. Zheng, R. Horstmeyer, and C. Yang, "Wide-field, high-resolution Fourier ptychographic microscopy," Nat. Photonics **7**, 739–745 (2013).
10. L. Tian and L. Waller, "3d intensity and phase imaging from light field measurements in an led array microscope," Optica **2**, 104–111 (2015).
11. F. M. Kahnert, "Numerical methods in electromagnetic scattering theory," J. Quant. Spect. Rad. Transf. **79–80**, 775–824 (2003).
12. R. Carminati, "Phase properties of the optical near field," Phys. Rev. E **55**, R4901–R4904 (1997).
13. B. Chen and J. J. Stamnes, "Validity of diffraction tomography based on the first Born and the first Rytov approximations," Appl. Opt. **37**, 2996–3006 (1998).
14. U. S. Kamilov, I. N. Papadopoulos, M. H. Shoreh, A. Goy, C. Vonesch, M. Unser, and D. Psaltis, "Learning approach to optical tomography," Optica **2**, 517–522 (2015).
15. P. C. Chaumet, A. Sentenac, and T. Zhang, "Reflection and transmission by large inhomogeneous media. Validity of Born, Rytov and beam propagation methods," J. Quant. Spectrosc. Radiat. Transf. **243**, 106816 (2020).
16. J. Lim, A. Wahab, G. Park, K. Lee, Y. Park, and J. C. Ye, "Beyond Born-Rytov limit for super-resolution optical diffraction tomography," Opt. Express **25**, 30445–30458 (2017).
17. H.-Y. Liu, D. Liu, H. Mansour, P. T. Boufounos, L. Waller, and U. S. Kamilov, "Seagle: Sparsity-driven image reconstruction under multiple scattering," IEEE Trans. Comput. Imaging **4**, 73–86 (2018).
18. T.-A. Pham, E. Soubies, A. Ayoub, J. Lim, D. Psaltis, and M. Unser, "Three-dimensional optical diffraction tomography with Lippmann-Schwinger model," IEEE Trans. Comput. Imaging **6**, 727–738 (2020).
19. M. Born and E. Wolf, *Principles of Optics* (Pergamon, 1959).
20. E. M. Purcell and C. R. Pennypacker, "Scattering and absorption of light by nonspherical dielectric grains," Astrophys. J. **186**, 705–714 (1973).
21. B. T. Draine, "The discrete-dipole approximation and its application to interstellar graphite grains," Astrophys. J. **333**, 848–872 (1988).
22. M. A. Yurkin and A. G. Hoekstra, "The discrete dipole approximation: An overview and recent developments," J. Quant. Spect. Rad. Transf. **106**, 558–589 (2007).
23. M. A. Yurkin, V. P. Maltsev, and A. G. Hoekstra, "The discrete dipole approximation for simulation of light scattering by particles much larger than the wavelength," J. Quant. Spect. Rad. Transf. **106**, 546–557 (2007).
24. P. C. Chaumet, D. Sentenac, G. Maire, M. Rasedujjaman, T. Zhang, and A. Sentenac, "IFDDA, an easy-to-use code for simulating the field scattered by 3d inhomogeneous objects in a stratified medium: tutorial," J. Opt. Soc. Am. A **38**, 1841–1852 (2021).
25. P. C. Chaumet and A. Rahmani, "Efficient iterative solution of the discrete dipole approximation for magneto- dielectric scatterers," Opt. Lett. **34**, 917–919 (2009).
26. P. J. Flatau, G. L. Stephens, and B. T. Draine, "Light scattering by rectangular solids in the discrete-dipole approximation: a new algorithm exploiting the Block-Toeplitz structure," J. Opt. Soc. Am. A **7**, 593–600 (1990).
27. P. C. Chaumet, T. Zhang, and A. Sentenac, "Fast far-field calculation in the discrete dipole approximation," J. Quant. Spectrosc. Radiat. Transf. **165**, 88–92 (2015).
28. B. T. Draine and P. J. Flatau, "Discrete-dipole approximation for scattering calculations," J. Opt. Soc. Am. A **11**, 1491–1499 (1994).
29. M. Paulus, P. Gay-Balmaz, and O. J. F. Martin, "Accurate and efficient computation of the Green's tensor for stratified media," Phys. Rev. E **62**, 5797–5807 (2000).
30. T. Zhang, C. Godavarthi, P. C. Chaumet, G. Maire, H. Giovannini, A. Talneau, M. Allain, K. Belkebir, and A. Sentenac, "Far-field diffraction microscopy at $\lambda/10$ resolution," Optica **3**, 609–612 (2016).
31. S. Shin, J. Eun, S. S. Lee, C. Lee, H. Hugonnet, D. K. Yoon, S.-H. Kim, T. Jeong, and Y. Park, "Tomographic measurement of dielectric tensors at optical frequency," Nat. Mater. **21**, 317–324 (2022).
32. P. C. Chaumet, A. Sentenac, and D. Sentenac, "Software IFDDA and IFDDAM," https://www.fresnel.fr/perso/chaumet/ifdda.html.